Journal of
Nuclear Medicine & Radiation Therapy

Vouche et al. J Nucl Med Radiat Ther 2011, 2:1
DOI: 10.4172/2155-9619.1000113

Special Issue Article Open Access

New Imaging Techniques for ^{90}Y Microsphere Radioembolization

Michaël Vouche[1], Bruno Vanderlinden[2], Philippe Delatte[1], Marc Lemort[1], Alain Hendlisz[3], Amélie Deleporte[3], Thomas Guiot[3], Camilo Garcia[3] and Patrick Flamen[3]*

[1]Department of Radiology, Jules Bordet Institute, Université Libre de Bruxelles, rue Héger-Bordet 1, B-1000 Brussels, Belgium
[2]Department of Medical Physicist, Jules Bordet Institute, Université Libre de Bruxelles, rue Héger-Bordet 1, B-1000 Brussels, Belgium
[3]Department of Nuclear Medecine, Jules Bordet Institute, Université Libre de Bruxelles, rue Héger-Bordet 1, B-1000 Brussels, Belgium
[4]Department of Digestive Oncology, Jules Bordet Institute, Université Libre de Bruxelles, rue Héger-Bordet 1, B-1000 Brussels, Belgium

Abstract

Adequate patient selection and treatment planning is crucial for a safe and cost-effective administration of selective internal radiotherapy (SIRT) of malignant liver disease using ^{90}Y-labelled microspheres. It requires the implementation of multimodality imaging, integrating metabolic, functional and structural characteristics. A multidisciplinary approach is a prerequisite for SIRT, bringing together the knowhow and expertise of radiologists, nuclear medicine physicians, medical physicists, imaging engineers, and radiotherapists. This review discusses the available radiologic (CT/MRI) and nuclear (SPECT/PET) imaging modalities and their specific utility in the different diagnostic phases related to SIRT: wholebody and intrahepatic pre-treatment disease staging, CT and MRI-based angiography, liver-lung shunt assessment, treatment simulation, predictive dosimetry, post-treatment imaging, and SIRT response assessment.

Keywords: Liver neoplasms; Microspheres; Yttrium Radioisotopes; Liver directed therapies; Multimodality Imaging

Abbreviations: SIRT: Selective Internal Radiotherapy; CT: Computed Tomography; MRI: Magnetic Resonance Imaging; SPECT: Single Photon Emission Computed Tomography; PET: Positron Emission Tomography

Introduction

The role of imaging in selective internal radiation therapy (SIRT) patient management is eminent both in patient selection and follow up. An adequate patient selection is crucial for a safe and cost-effective implementation of SIRT. Imaging will mostly perform a negative selection for SIRT: via the identification of patients with liver tumors that will not have a prognostic benefit from SIRT because of inappropriate disease stage (high extrahepatic tumor load impairing short term prognosis) or tumor characteristics (liver tumors with a low arterial supply) or because of toxicity risk (extrahepatic microsphere deposition via aberrant arteries that cannot be properly embolized prior to SIRT; arteriovenous shunting leading to potentially high radiation dose to the lungs; radioembolization induced liver disease).

All this requires the sequential implementation and integration of diagnostic information obtained with both structural and metabolic diagnostic tools. The integration of data has been recently facilitated through the advent of multimodality tools, combining, in one camera gantry, metabolic or molecular imaging (PET or SPECT) with a structural or morphological imaging tool (CT or MRI), the so-called "hybrid systems". Imaging data integration requires a fundamental multidisciplinary approach bringing together the knowhow and expertise of radiologists, nuclear medicine physicians, medical physicists, imaging engineers, and radiotherapists.

This review will discuss the current state of the art of imaging in the different aspects of the management of patients undergoing SIRT.

Pre-treatment tumor extension assessment

The choice of the pre-treatment imaging modality is a critical point in the management of SIRT patients. It is crucial to choose a technique that allows the most accurate assessment of the intra- and extra-hepatic tumor load. Generally, SIRT is not indicated in case of major uncontrolled extra-hepatic disease which could impair the prognostic benefit yielded by SIRT. Extra-hepatic disease might be accepted when it is considered as responsive to systemic or other local therapies associated to the SIRT within a multimodality therapeutic strategy. Thus, for pre-SIRT imaging of tumors with high propensity for systemic metastases (colorectal cancer; breast cancer; cholangiocarcinoma) high sensitive whole body imaging techniques are preferred (FDG PET-CT). Secondly, hepatic pre-SIRT imaging should be accurate, both in terms of sensitivity (accurate liver tumor mapping, important for SIRT treatment planning: supraselective approach versus global liver treatment) as specificity. Specificity is important because most of our patients are scheduled for SIRT after previous cytotoxic or locally ablative or surgical interventions. In these conditions it might be difficult to differentiate aspecific treatment induced changes (fibrosis / necrosis) from residual or recurrent tumor. For this, it is indicated to use a functional (MRI) or metabolic (PET/CT) imaging technique with image findings being more related to tumoral viability rather than tissue density. Thirdly, the pre-SIRT imaging technique of choice will serve as a baseline tumor status to which later scans will be compared to assess SIRT response and residual disease. Therefore, the technique should be sensitive to measure antitumoral effects of SIRT, allowing rapid identification of lesions with poor or absent response that could benefit from additional local therapy such as radiofrequency ablation of selective external beam radiotherapy.

For all these reasons, as a baseline pre-SIRT examination, the perfect imaging modality would consist in a secure, fast, widely

***Corresponding author:** Patrick Flamen, Department of Nuclear Medecine, Jules Bordet Institute, Université Libre de Bruxelles, rue Héger-Bordet 1, B-1000 Brussels, Belgium, E-mail: patrick.flamen@bordet.be

Received April 26, 2011; **Accepted** May 26, 2011; **Published** June 15, 2011

Citation: Vouche M, Vanderlinden B, Delatte P, Lemort M, Hendlisz A, et al. (2011) New Imaging Techniques for ^{90}Y Microsphere Radioembolization. J Nucl Med Radiat Ther 2:113. doi:10.4172/2155-9619.1000113

available and relatively low-cost technique, covering the entire body with high performances in terms of sensitivity and specificity.

Whole body PET-CT, using tumor tracers labelled by a positron-emitting isotope (18F or 68Ga), is a most suitable imaging modality. The imaging basis of FDG PET-CT is the high glycolysis rate observed in most tumors, which leads to an intense accumulation of FDG via an increased expression of cell membrane glucose transporters (GLUT) and hexokinase (the latter transfers FDG to FDG-6-phosphate) and a low rate of dephosphatase activity. This is the case in most recurrent colorectal and breast carcinoma, to name two frequent tumors often sent to our department for evaluating the possibility for SIRT. However, some neoplasms referred for SIRT are known to show low or inconstant FDG avidity. These include low-grade tumors (eg. low proliferating neuroendocrine tumors), tumors with a high phosphatase activity (leading to a wash out of the intracellular FDG; which is the case in well differentiated hepatocellular carcinoma), tumors with a high mucinous content (some mucinous colorectal and gastric tumors). In these tumors, when sent for SIRT, pretreatment FDG PET-CT should not be routinely performed and other metabolic or functional diagnostic tools should be considered (111In or 68Ga labelled octreotide; functional MRI).

It should always be kept in mind that non-tumoral conditions can show high FDG uptake mimicking neoplastic activity. False positive findings in liver parenchyma can occur in cases of granulation tissue (e.g., at the resection planes after hepatic surgery), inflammation (eg. after radiophrequency ablation), and infections (abcesses; tropical diseases). On the other hand, recent chemo/radiotherapy can supress tumor metabolism partially or even completely without eradication of the tumoral activity. Therefore, pre-SIRT PET-CT should be performed in case of clinically chemo-refractory disease, or, in case of effective chemotherapy, after stopping it during several weeks. Anyway, performing SIRT in patients responding to chemotherapy is probably not indicated because response is often associated with a drop of arterial vascularisation, which is the major basis for successful SIRT.

The most common indications for SIRT are hepatocellular carcinoma (HCC), liver metastatic colorectal cancer (CRC), intrahepatic cholangiocarcinoma, and neuroendocrine tumors. Increasing numbers of patients with liver only recurrent breast cancer or (ocular) melanoma are reported [1-3]. The tumor specific pitfalls and recommendations regarding pre-SIRT imaging are discussed here under.

Liver dominant CRC metastasis: First-line follow-up and assessment of recurrent CRC is classically performed by (combinations of) liver ultrasound (US), Contrast Enhanced-CT (CECT) or MR. In case of diagnostic need (eg. increasing tumor markers with normal imaging, or equivocal CT/MRI findings) FDG PET-CT is generally performed because of its higher whole body sensitivity and specificity [4,5]. FDG PET-CT has now been proved to be significantly more accurate than ce-CT for diagnosis of hepatic metastasis, and equivalent or somewhat lower to liver MRI [6-8].

FDG PET has less spatial resolution compared to the structural cross sectional imaging modalities such as CT and MRI. Therefore, small infracentimetric hepatic lesions are still not easily detected on FDG PET due to relatively high and heterogeneous physiological background liver activity. However, the low specificity of CECT and MRI for these lesions still poses a significant clinical problem, and may requires the use of more specific dedicated MRI tools such as contrast-enhanced or diffusion-weighted imaging [9,10]. For the contrast enhanced MRI, Super Paramagnetic Iron Oxides (SPIO) have now been proved to be at least as accurate than Gadolinium (Gd) for differentiating malignant from benign hepatic masses or adjacent nodes [11-13].

Sometimes CRC metastases have a high mucinous content with low cellularity. These tumors have a low avidity of FDG and FDG PET-CT can therefore significantly underestimate the liver disease extent. In this condition FDG PET should not be used for pre- or post-SIRT disease evaluation.

Hepatocellular cancer: FDG PET-CT is not routinely performed in HCC because of the fact that only about 30% of HCC are FDG avid [14] (Figure 1). This leads to a significant underestimation of the disease extent. The reason for the non-avidity for FDG is the high glucose-6-phosphatase activity present in these tumors, which leads to a non-accumulation of FDG in the tumor cells. Only dedifferentiated, more aggressive HCC cells lose this enzyme overexpression and show more intense FDG uptake. It has been observed that HCCs with higher FDG uptake have a higher tendency for extrahepatic metastases than those with lower FDG uptake [15]. Further observational studies will teach us how this could be used for the prognostic stratification of patients with HCC.

HCC occurs preferentially on cirrhotic and altered liver parenchyma rendering structural imaging modalities (CT/MRI) not accurate enough for the characterization of small lesions. Moreover, the radiological findings are often inconsistent and subtle [16]. Therefore, early diagnosis and proper staging is still challenging and different scoring and classification systems are reported, including primary tumor size and extension, portal vein thrombosis, regional lymph node involvement, the presence of distant metastasis, the histological grade and the degree of fibrosis [17].

MRI and CECT (Figure 1), on morphological basis, have similar performances for the detection of intra- and extra-hepatic HCC, and both techniques are equally sensitive for the detection of lesions measuring 2 cm or larger but insensitive for HCC lesions smaller than 2 cm, and for carcinomatosis [18,19]. Recent recommendations by the American Association for the Study of Liver Diseases state that a diagnosis of HCC can be made if a mass larger than 2 cm shows typical features of HCC (hypervascularity in the arterial phase and washout in the venous phase) at CECT or MRI, or if a mass measuring 1-2 cm shows these features at both modalities [20]. Even if not entirely discriminating, the Diffusion-Weighted MRI does provide additional information for suspicious lesions (Figure 1). It improves MRI detection of HCC, particularly in lesions smaller than 2cm, with sensitivities of 84-98% compared to 76-85% for multiphasic MRI alone [21-23].

The place of other molecular imaging biomarkers is currently being evaluated, such as the18F-fluorocholine or 11C-acetate [24]. Also, some of these tumors have a high expression of somatostatine receptors and might therefore be imaged using radiolabelled octreotide and PET-CT or SPECT-CT (see lower).

Neuroendocrine tumors: Neuroendocrine tumors (NET) can show neuroamine uptake or cell membrane somatostatine receptors; both biomarkers can be used for molecular imaging using targeted radiolabelled ligands. The oldest ligand that was developed is MIBG (metaiodobenzylguanidine), which is a substrate of the neuroamine uptake. MIBG imaging does not play a role anymore for intra or extrahepatic staging of NET because of the relative poor imaging characteristics of 131I-SPECT and of its high cost and radiation burden for the patient. MIBG imaging is still used to select NET patients

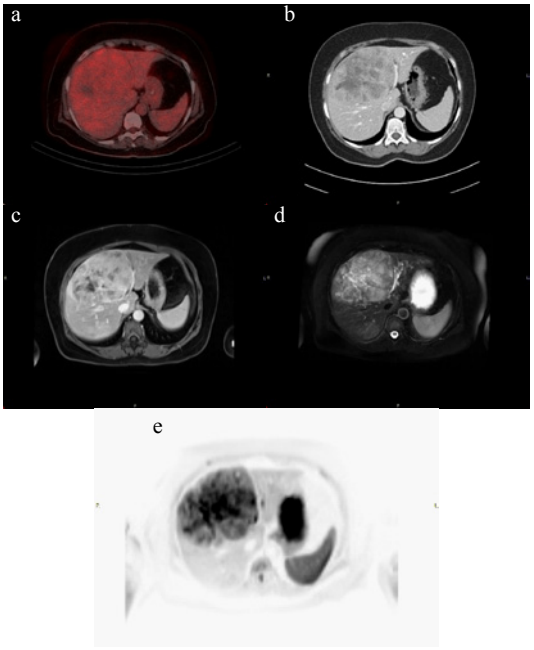

Figure 1: Registered axial images of patient with a large HCC lesion in the right liver lobe: FDG PET-CT (a), portal phase CECT (b), fat suppression Gd enhanced T1w MRI (c), fat suppression T2w MRI (d), and DWI b800 MRI (e). Note that FDG PET-CT does not show any tracer accumulation in the tumor lesion (non avidity). MRI provides the best tumor to normal liver contrast.

who might benefit from metabolically targeted radiotherapy through the intravenous administration of high activity of 131I-MIBG. This treatment can be an adjunct to SIRT in case of the presence of hepatic and extrahepatic disease sites, but is probably less effective (but more available) than treatments using radiolabelled octreotide.

The primary molecular imaging tool is based upon the high expression of somatostatine receptors in NET. Octreotide, a small peptide, targets the receptor and can be labelled with isotopes for both SPECT (111In) and PET (68Ga) imaging.

In most European oncology imaging centers Octreoscan (111In-pentetreotide), using gamma camera-based planar and SPECT imaging (performed at 6, 24 and sometimes also 48 hours after tracer administration), is gradually being replaced by 68Ga-octreotide PET-CT (performed at 1h30 post tracer administration), because of PET's better sensitivity (about 2000 times higher than SPECT) and 3D spatial resolution (6-8 mm for PET compared to 12-14 mm for SPECT [25,26]. The success of the so-called "Octreo-PET" has been facilitated by the commercial availability of 68Ge-68Ga generators with an acceptable cost and long shelf-life (1 year or longer). This allows the home-made production of the radiotracer using dedicated (semi)automated radiosynthesis modules. Another indication for octreotide-based imaging is the selection of patients for radiolabelled octreotide systemic treatments, using therapeutic B-emitting isotopes such as Yttrium-90 and Lutetium-177. This treatment modality can be an important adjunct for SIRT in case of extrahepatic disease. In this situation we mostly perform first the liver SIRT in order to downstage liver disease (which often is the primary source of the clinical neuro-endocrine syndrome), followed by the systemic radionuclide treatment.

The uptake of FDG in well differentiated, low grade NET (carcinoids) is often not increased. However, it has been reported that the uptake of FDG increases with the proliferation rate and degree of differentiation of NET [27,28]. Therefore, FDG PET-CT can have a major role in non-invasive "grading" of the NET sites. Whole body FDG PET is also important to indicate the site for the most appropriate biopsy, the hottest lesion being the most relevant in terms of prognosis. For the planning of SIRT in multimetastatic NET, FDG PET-CT should be routinely used to grade the extrahepatic disease (Figure 2). Absence of FDG indicates low grade lesions which will mostly not become prognostically relevant in the coming months/years, while FDG positive lesions outside the liver should be considered as a relative contra-indication for liver SIRT.

Cholangiocarcinoma : Staging cholangiocarcinoma is a major challenge. This neoplasm, deriving from the biliary ducts, is subdivised in 3 types: intra-hepatic, peri-hilar and extra-hepatic type. Distant metastasis can involve lymph nodes (50% at presentation), peritoneal cavity or distant organs (10-20% at presentation) [24]. Prognosis of patients with non resectable cholangiocarcinoma is generally unfavourable. Therefore, the indication of SIRT in these patients should be restricted to the liver-exclusive disease in whom high SIRT radiation doses can be obtained, preferably in a supraselective (ablative) approach (see lower Predictive Dosimetry).

Cholangiocarcinomas are usually detected on multiphase CECT. After the intravenous administration of contrast material, most cholangiocarcinoma remain hypoattenuating during the arterial and portal venous phases and show enhancement during the delayed phase, findings that reflect their hypovascular desmoplastic composition. In addition to providing valuable information regarding local disease, multidetector CT helps scrutinize the entire abdomen and pelvis for metastatic spread to lymph nodes and distant organs, although the sensitivity of CT for lymph node metastases has been found to be low (about 50%) [25].

MRI, providing superior contrast resolution, enhancement kinetic study, diffusion-weighted imaging and non-invasive cholangiography, is superior to CECT for the assessment of intraductal, satellite or small lesions. The intra-hepatic involvement assessment should therefore preferentially be made by MRI. However, MRI sensitivity in the detection of distant metastasis is poor because of limited field of view and false negative findings due to small lesion size [26].

Little is known about the use of FDG PET-CT in cholangiocarcinoma. FDG PET seems to be more useful in detecting metastases to lymph nodes, the liver, and other distant sites compared to conventional staging techniques. However, in patients that underwent extensive conventional and laparoscopic staging, a recent study in 30 intrahepatic

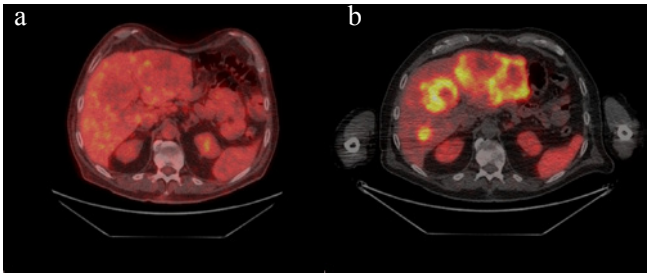

Figure 2: Registered axial images of patient with multiple metastases of a low-grade neuro-endocrine tumor. FDG PET-CT (a) does not show any increased FDG avidity (indicative for a low grade tumor), while 68Ga-Octreotate PET-CT (b) shows high tumor tracer uptake due to the increased expression of the somatostatin receptors.

cholangiocarcinoma patients indicated that FDG PET-CT does not provide any significant additional information [26-28].

Intra- and perihepatic investigation by PET, CT and MR is complicated by overlaps of positive findings of cholangiocarcinoma and inflammatory biliary strictures in case of sclerotising cholangitis, which is a preponderant pathology for the development of cholangiocarcinoma. Moreover, infiltrating cholangiocarcinoma is less precisely delineated and detected than nodular types.

SIRT simulation

Before SIRT, a treatment simulation with 99mTc-labeled MAA particles should be performed in order to exclude the presence of lung shunting, to assess the intrahepatic distribution, and to detect undesirable extrahepatic spread of the injected microspheres.

The images obtained during the 99mTc-MAA-simulation procedures are crucial for SIRT treatment planning and predictive dosimetry. Therefore, it is essential that the catheter tip during the 99mTc-MAA injection be positioned in the anticipated SIRT treatment position in order to maximally assure a comparable distribution of the 99mTc-MAA and the SIRT particles.

Therefore, before simulation, a dedicated CT or MRI-angiography should be performed in order to plan the most appropriate catheter placement and to detect vasculature abnormalities or variants of the arteries supplying the liver [30]. Two modalities available for pre-simulation imaging (CT and MRI based angiography) are briefly discussed hereunder.

CT angiography: Recent improvements of multidetector-CT now permit to explore the entire abdominal and limbs vasculature in one single breath hold. Volumetric data acquisition and multiphase imaging offer the possibility to depict the catheterism access way, the liver arterial vasculature conformation, and the characterization of the tumor vascularization. The angio-CT findings are now very reliable and offer a good correlation with digital subtraction angiography (DSA), which remains the gold standard in assessing liver vasculature and tumor feeding arteries [31-35].

The classical angio-CT protocols include the injection of 150 mL of non-ionic iodinated contrast material with a high concentration of iodine (300-400 mg per milliliter) through an 18-20-gauge intravenous cannula at a high flow rate (about 5 mL/sec if possible).

The delay of the hepatic arterial phase scan is about 20 -25 seconds while the portal venous time is 60-65 sec after the administration of iodinated contrast agent. The ideal irradiation parameter should be 120 kVp; and 220 --260 mA [36].

Post-processing tools now permit to perform 3D multiplanar reconstructions and to delineate precisely the entire aortic trunk and the feeding aortic branches of the liver with the use of maximal intensity projection (MIP), shaded-surface display (SSD) and volume rendering (VR) settings tools.

Angio-CT requires high speed imaging acquisition and thus the use of multidetector CT which may induce cone beam artifacts. Moreover, metallic artifacts due to previous surgical procedures on the liver can complicate the interpretation of the images. High flow rate injection of iodinated contrast agents can be problematic with patients with bad venous conditions. Finally, angio-CT delivers a relatively high amount of ionizing radiation (CTDI vol about 30,0 mGy for an abdominal angio-CT [37]), but radiation risk considerations should of course be balanced against the prognosis of the disease and the patient's life expectancy.

Gadolinium-enhanced MR Angiography: Gadolinium-enhanced (Gde) MRI angiography has been established as a safe, accurate, noninvasive method for evaluating the hepatic vasculature. Fast and high spatial-resolution angiographic imaging is now possible. Isometric acquisitions can be achieved, resulting in 3D multiplanar reconstruction possibilities. Gde-MRI can depict hepatic vessels with a good resolution with low saturation or turbulence-related artifacts. Moreover, compared to the angio-CT, Gde-MRI angiography is not ionizing, and rarely causes hypersensitivity reactions.

Gde-MRI angiography sequences can be added to the usual morphologic breath-hold T1-weighted in-phase and opposed-phase gradient-echo images and T2-weighted images of the liver.

The Gde sequences include an axial breath-hold 3D interpolated spoiled gradient-echo sequence after intravenous administration of gadolinium chelate (40ml) injected at a flow rate of 2 ml/sec, which is quite lower than flows used for angio-CT.

Hepatic arterial and portal venous phase images are obtained after a delay of 15-18 seconds and 70 seconds, respectively. Breath-hold images are obtained at end inspiration and usually require less than 30 seconds. As for the angio-CT, 3D multiplanar acquisitions permit maximum intensity projection (MIP) and volume rendering (VR) reconstruction, which are most useful in the SIRT simulation planning (Figure 3).

The visualization of small vessels is often mandatory to properly plan the SIRT catheter placement. Despite major improvements of angiographic sequences and the increasing availability of powerful magnets (1,5 and 3 Tesla), the spatial resolution of MR angiography is still inferior to that of angio-CT and DSA [38]. Moreover, long breath-hold sequences may be spoiled by motion artifacts in patients with bad respiratory conditions.

For these reasons, and if no contra-indication is present, the preferred modality for the pre-simulation imaging should be angio-CT. Both modalities do offer correct visualization of the liver arterial vasculature [39] but only angio-CT permit to depict the tumor arterial vasculature almost as precisely as the DSA (Figure 3).

Digital subtraction angiography and added value of cone beam CT: DSA has been used for decades by interventional radiologists. It consists of a fluoroscopy system disposed on a C-arm permitting rotation around the patient table. It permits the clear visualization of blood vessels in a bony or dense soft tissue environment. Images

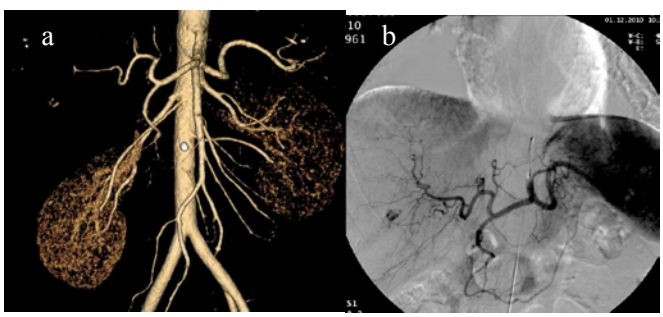

Figure 3: 3D rendering of a CECT (a) and the corresponding DSA (b) anterior view, illustrating the higher resolution of DSA with a much better visualization of small vessels.

are produced using iodinated contrast medium by subtracting a 'pre-contrast image' (mask) from later images, once the contrast medium has been introduced into a structure.

The recent development of the Cone Beam Computed Tomography technology (CBCT) now offers new perspectives for interventional oncology of the liver.

It is composed by a silicium flat-panel fluoroscopy system incorporated in a C-arm device, which allows 360° rotation around the interventional table. It provides tomographic CT-like images in addition to the planar angiographic data. It is complementary to the classical DSA, providing better tumor vasculature depiction and detecting shunting arterioles that were not seen on DSA. Despite frequent metallic and beam hardening artifacts due to previous surgery, bowel gas or catheter positioning, CBCT uses cross sectional technology acquisition with 3D reconstructions, and is consequently not prone to superposition artifacts.

Added value of the CBCT has already been demonstrated for liver chemoembolization, improving catheter placement and the confidence for the selection of the arteriole to embolize [40,41]. While using equivalent contrast agent amount during a CBCT acquisition compared to DSA, irradiation dose appears to be inferior to DSA, due to inferior amperage, which is a major advantage for the angiographist [42].

The detection and subsequent coil embolization of extra hepatic shunting to other gastro-intestinal structures is a major issue during SIRT simulation angiography [43,44]. According to Louie et al. [45], the high spatial resolution of CBCT supplements the traditional use of DSA and 99mTc-MAA scintigraphy to predict extrahepatic microsphere deposition. Most importantly, CBCT can help to spare non-tumoral liver parenchyma by detecting the feeding arterioles of the targeted tumors and to ensure a selective or even supra-selective catheter positioning. In a recent study of Louie et al. [45], the CBCT findings during SIRT simulation convinced angiographists to perform an additional embolization or to change the catheter positioning in 33% of cases, because of the risk for non-target embolization or incomplete tumor perfusion not seen on DSA. For these reasons incorporating CBCT technology in the SIRT simulation and treatment phase constitutes a major progress for patient safety and treatment optimization.

99mTc-MAA planar or Single Photon Emission Computed Tomography (SPECT)

The simulation of the proper distribution of Yttrium-loaded microspheres within and outside the liver is mandatory to ensure a safe SIRT procedure. This simulation can be performed through the infusion of Macro-Aggregate of Albumine labelled with 99mTc (99mTc-MAA) after intravascular catheter placement in the liver arterial vasculature. Photons emitted by the 99mTc can be detected by planar or 3D single photon detectors (SPECT) using gamma-cameras. Whereas planar images are sufficient to estimate the lung shunt, the estimation of the microspheres distribution inside the liver must be assessed tomographically using SPECT [46]. Moreover, the use of a hybrid system (SPECT-CT) has proven useful for image registration and delineation [47]. 99mTc-MAA SPECT images should be performed as soon as possible after administration of the radiotracer (usual activity: 150-300 MBq) because free 99mTc can enter the system circulation and fix itself in the gastric mucosa. This extrahepatic activity cannot be differentiated from deposition coming from aberrant extrahepatic arteries. Because the presence of free Tc99m is variable and unpredictable, it is generally recommended to pre-administer a dose of percholrate (Irenate) which completely blocks the uptake of free Tc99m in the gastric mucosa. The pharmacologic effect of the drug can be checked by verifying the absence of any physiological uptake seen in the thyroid (Figure 5). In our center, Perchlorate is administered routinely, about 20 minutes before the 99mTc-MAA administration (i.e. right before starting the catheterization).

In some patients, when supraselective SIRT approach is indicated, or when preSIRT embolization of a gastro-duodenal artery is technically impossible, 2 doses of 99mTc-MAA are injected separately in both hepatic arteries.

Image processing

Activity dosing for SIRT should be based on the patient and tumor-specific conditions, such as whole liver volume, treated liver volume, tumor volume, lung shunting, and arterial hypervascularization of each tumors. These parameters can be measured (or approximated) before SIRT by integrating information from dedicated multimodality imaging which requires advanced image processing.

First, a method for image registration and lesion delineation should be defined. There is currently no standard or consensus methodology for this. The preferred method should have minimal inter- and intraobserver variability leading to the highest achievable clinical standardization. Hereunder are presented some aspects of the methodology presently used in clinical SIRT routine at the Jules Bordet Institute.

Image registration: Image registration is necessary in order to be able to compare or integrate the data obtained from different image-based measurements. For this, each image is transformed so that all are in the same spatial coordinate system. The reference coordinate is "the clinical reference image" corresponding to the baseline image depicting the SIRT target lesions. So, the 99mTc-99mTc-MAA SPECT images, and later the post-treatment images (and potentially the treatment response images) will all be registered in the space of that reference image (Figure 4).

The registration of anatomic and metabolic images can be complicated because of the different information content. The use of hybrid systems (SPECT-CT or PET-CT) simplifies the process because only the anatomic images need to be registered; the same registration transformation is then applied to the associated metabolic images. However, local movements such as breathing and heartbeats can sometimes give a mismatch between anatomic and metabolic images (even in hybrid systems) resulting in artifacts that are difficult to

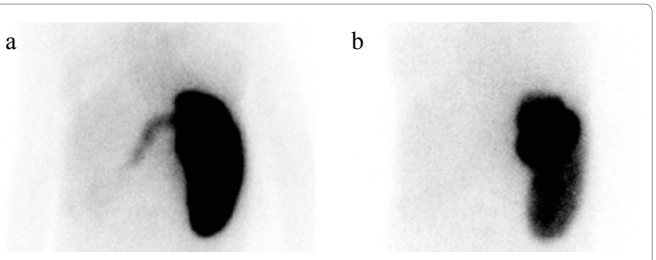

Figure 4: Anterior view of the Maximum Intensity Projection of 99mTc-MAA SPECT of a same patient who underwent two 99mTc-MAA-simulations before SIRT of a spleen : without (a) and with (b) prior oral administration of perchlorate. The physiological uptake of free 99mTc seen in the gastroduodenal wall is completely supressed by the perchlorate.

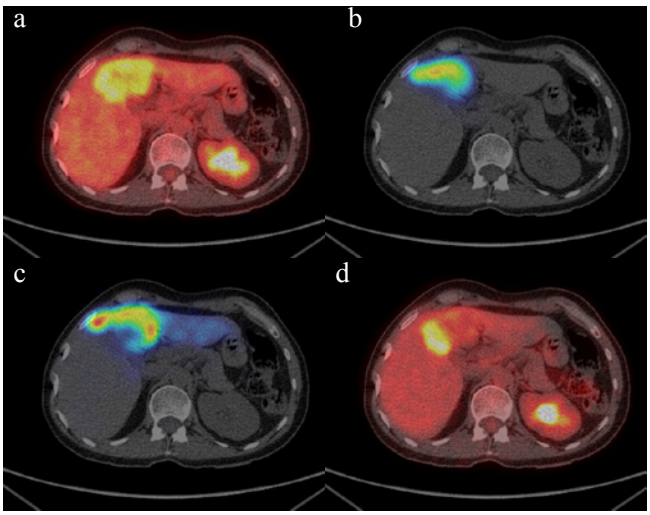

Figure 5: Registered axial images of a patient with liver metastatic colorectal cancer. (a) baseline FDG PET-CT shows the target lesion with central necrosis located in segment IV,(b) simulation SPECT-CT image after supraselective 99Tc-MAA administration in the left hepatic artery, indicating that the lateral part of the lesion is not perfused via the left hepatic artery; (c) the post-treatment 90Y PET-CT after supraselective SIRT administered in the left hepatic artery, showing microsphere deposition in the peripherical (non-necrotic) part of the lesion, except for the lateral part, confirming the 99mTc-MAA SPECT-CT finding ; (d) FDG PET-CT image obtained at 6 weeks post SIRT indicating residual (non-treated) disease at the lateral segment of the initial tumor. The medial part of the lesion shows an almost complete metabolic response. Additional local ablative treatment of the residual tumor lesion was needed.

correct. Therefore, these must always be taken into account by visually assessing the quality of the matching between the registered images.

The most advanced registration is the registration of 3D angiographic images (angio-CT or angio-MRI) with the reference images. This enables to define the different arteries perfusing the different lesions and can help to define the best location to position the catheter for SIRT simulation and treatment (Figure 3). However, this method still is limited by the poor resolution of the angiographic images.

Delineation of organs and lesions: 3.2.1. Lung shunt: To estimate the lung shunt, regions of interest (ROI) on the lungs and liver should be generated on the planar 99mTc-MAA-scan. Three ROIs are defined: one liver ROI on the anterior image, and two lungs ROIs on the posterior 99mTc-MAA images. For lung delineation, the posterior images are preferred because of the heart attenuation present on anterior images. For reasons of reproducibility, we perform a threshold segmentation based on a percentage of the maximum value inside each ROI. These ROIs are then mirrored to be projected on the conjugated anterior (lungs) or posterior (liver) images. At the end, we have six regions that allow us to calculate the geometric means inside the liver and lungs, and compute the percentage of shunting (Figure 6). Because of different artefacts between liver and lungs (e.g. attenuation and scatter), this method overestimates the shunt. For a more proper quantification of the shunt, leading to more accurate dosimetry calculations, the EANM guidelines recommend to use SPECT-CT [48] however without providing a standardized methodology.

Liver and lesion delineation: A SIRT dosimetry, or any other quantification, requires the definition of the target volumes and the estimation of activity within these volumes. The whole liver volume must be defined on anatomic images (CT/MRI). However, the target tumor lesions must be defined on the clinical reference images. If the clinical reference image is MRI or CT, an automated segmentation or manual definition should be applied. However, accurate lesion delineation is often difficult because of lack of tumor specificity of structural imaging (see higher). On the other hand,,the delineation of tumor lesions on metabolic images is highly dependant on the user, the software and the resolution of the images.

In our centre, we perform segmentation of the FDG PET lesions by using a threshold of twice the normal liver parenchyma uptake.

The liver and tumor regions can then be projected on the registered 99mTc-MAA-SPECT in order to quantify the tumour to non-tumour contrast. This quantification can then be used for obtaining a predictive SIRT dosimetry on a lesion by lesion basis, as reported by Flamen et al. [49] which is most informative when discussing a multimodality approach for liver tumors.

Post treatment imaging

The distribution of ^{90}Y microspheres should be imaged routinely in order to assess the accurate delivery of the treatment in terms of treatment field, extrahepatic deposition and tumor to non-tumor accumulation. Moreover, the quantification of these images could enable to calculate the real dosimetry of the treatment. The currently available techniques using gamma camera and PET technology are discussed hereunder.

^{90}Y bremsstrahlung planar imaging: The spectrum of electrons emitted by the ^{90}Y can be indirectly imaged through the principle of Bremsstrahlung ("braking radiation"). Bremsstrahlung is generated when fast-moving electrons closely approach atomic nuclei and are deflected of their incident trajectory by electrostatic forces (Figure 7). The energy loss due to this deflection is emitted in the form of photon radiations. Since the delta of energy due to deflection differs in function of the path of the incident electron, Brehmsstrahlung essentially produces a continuous photon spectrum (Figure 8).

Imaging a continuous photon energy spectrum is unusual in nuclear medicine imaging and results in an increase of artefacts and loss of image quality.

Gamma cameras use collimators to absorb photons whose trajectory is not perpendicular to the camera. The choice of collimator type results from a compromise between the energy of photons that are well attenuated, the spatial resolution and the detection sensitivity.

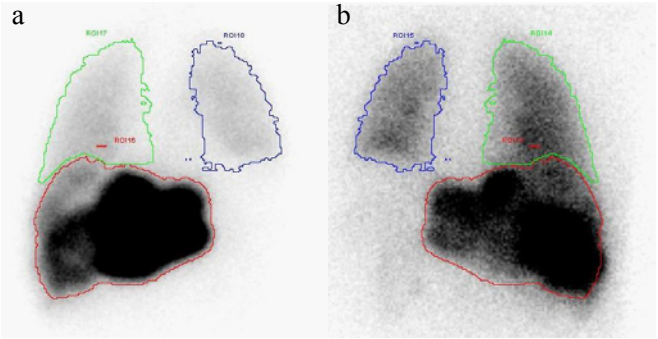

Figure 6: Planar Anterior (a) and Posterior (b) image of SIRT simulation with 99mTc-MAA showing a significant liver-lung shunt (19% of the injected 99mTc-MAA activity) and the ROIs used for his estimation.

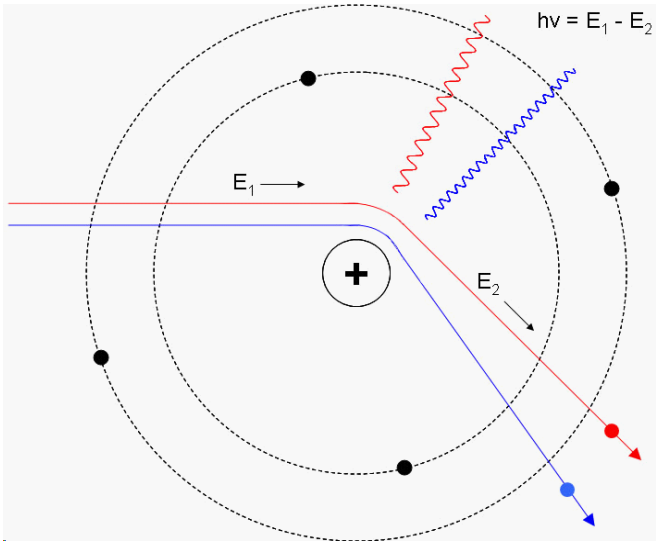

Figure 7: Bremsstrahlung is generated when fast-moving electrons (blue and red lines) closely approach atomic nuclei and are deflected of their incident trajectory by electrostatic forces. The energy loss due to this deflection is emitted in the form of photon radiations.

Conventional gamma imaging selects photons of energy that correspond to a range of 20% around the energy of the photon emitted by the source (e.g. 140 keV for 99mTc). The range of energy photons accepted is defined by the energy window (e.g. [126-154] keV for 99mTc). This selection enables the elimination of most of scattered photons because they have lost some of their energy. It is important to eliminate the scattered photons because they blur the image and thereby decrease the contrast of the image. With Bremsstrahlung imaging, the direct and scattered photons are mixed, so the discrimination can not be done with the definition of the energy window. However, the selection of a specific photon energy window at image acquisition as well as the choice of the collimator can significantly improve image quality.

Already in 1994, Sui Shen et al. [50] studied the impact of the choice of the energy window and collimator on planar Bremsstrahlung imaging in terms of resolution and sensitivity [50].

Based upon this standard work, it was recommended to use a medium energy collimator and acquire two simultaneous images with energy windows set at [50-150] keV and [151-300] keV. In our experience (Figure 9), the images obtained in the high energy window contain more artefacts, but they can be summed to the low energy image if more sensitivity is required. With these parameters Shen et al.[51] performed planar quantification experiments and concluded that reasonably accurate quantification of 90Y was achievable using gamma camera imaging which could serve as a basis of radiation dose estimation.

^{90}Y Bremsstrahlung Emission Computed Tomography (BECT): As for SIRT simulation, the use of tomography increases the usefulness of the imaging. Since emission computed tomography is reconstructed through planar images, the issues inherent to planar imaging (choice of collimators and energy windows) are still relevant to BECT. However an additional issue with BECT is the attenuation correction.

Attenuation correction depends both on the density of objects through which the photon pass, and on the photon's energy. For a given density, photons with higher energy will be less attenuated than photons with lower energy. Usually, attenuation correction is computed from CT images where the Hounsfield values are converted to attenuation coefficients of the specific energy of the acquired photon (e.g. 140 keV for 99mTc, or 511 keV for a positron emitter). Theoretically, for Bremsstrahlung imaging with its continuous energy spectrum, different energy windows are needed in order to compute different attenuation coefficients.

Ito et al. [52] performed a phantom study to investigate all the problems inherent to BECT. Their choice of collimators was the same as for planar imaging, but they proposed three energy windows with the following widths: 50% (57-94 keV) centered at 75 keV, 30% (102-138 keV) at 120 keV, and 50% (139-232 keV) at 185 keV [52].

Other groups studied BECT quantification and they all concluded that it is achievable [53] and [54]. However, presently, there still is no reference consensus for BECT based SIRT dosimetry in clinical routine.

In these circumstances, we currently assess the SIRT dosimetry via the pre-SIRT dosimetry model computed from the 99mTc-MAA simulation. Of course, this is only valid when the 3D distribution of 99mTc-MAA and the SIRT microspheres are identical, which should be assessed by registrating the BECT with the 99mTc-MAA-SPECT images.

^{90}Y Positron emission tomography: ^{90}Y is traditionally considered as a pure beta emitter, decaying to 90-Zirconium (Zr) with a transition energy of 2.26 MeV. However, this decay branch is not unique. In fact, it has been shown that a small proportion of 90Y decays to an excited state of 90Zr. The desexcitation that follows consists in the emission of either a conversion electron or an internal pair creation. The latter leads to the emission of positrons. The internal pair production branching ratio of 90Y has been determined to be 3.186 x 10-5 [55] (Figure 10).

Despite this poor ratio, the increased detection sensitivity of the latest generation PET technology, using Time of Flight (TOF) correction, can acquire the photons generated by the positron annihilation [56]. Later, the same group proved that this image could be quantified and thus be useful for post SIRT dosimetry [57]. With our scanner (General Electric; Discovery D690) we consider that for the amount of Sirsphere (1-3 GBq) injected, each bed position acquisition must at least last 30 minutes in order to obtain acceptable results

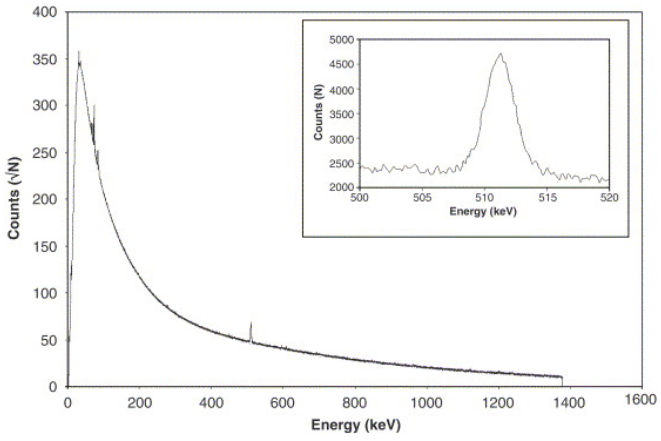

Figure 8: A typical germanium spectrum from 90Sr/90Y after background subtraction. The embedded plot is an enlarged portion of the 511 keV peak resulting from positron emission, allowing PET imaging.

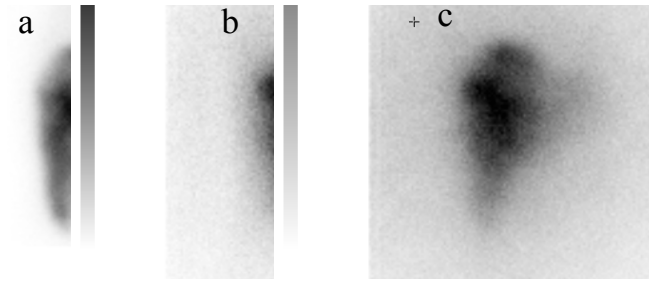

Figure 9: (a) Anterior image of SIRT simulation with 99mTc-MAA. Anterior image of SIRT during treatment acquired with an energy window: (b) [52.5 87.5] KeV and (c) [97.0 287.4] KeV

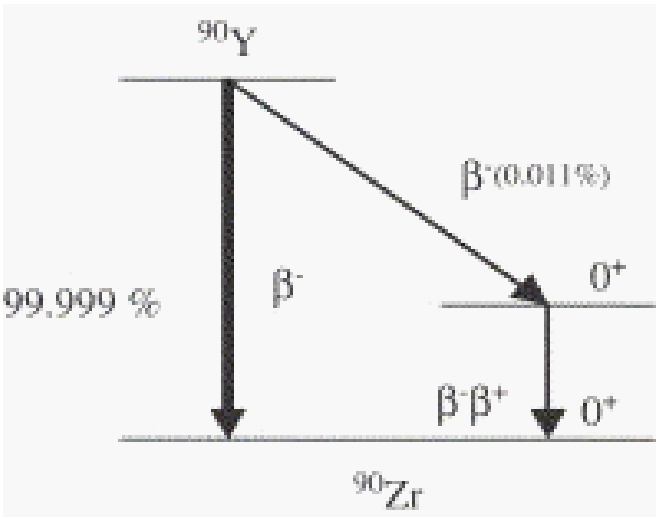

Figure 10: Decay scheme of ^{90}Y.

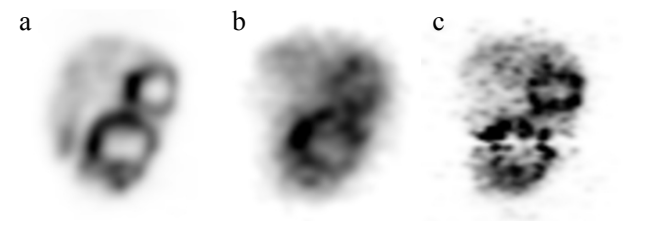

Figure 11: Registered sagital images of SIRT simulation with 99mTc-MAA SPECT (a), 90Y BECT (b) and PET (c).

(Figure 11). Because the axial coverage of a PET bed position is only 15 cm, imaging a whole liver takes at least one hour, compared to about 30 minutes with BECT imaging.

SIRT response assessment

Early assessment of response post SIRT should be performed for prognostic evaluation and for allowing rapid treatment adaptation when (part) of targeted tumor load is not or poorly responding. In the latter conditions SIRT can be associated to other locally ablative therapies such as radiofrequency ablation or volume selective external beam radiotherapy (eg. Cyberknife).

SIRT induces specific changes in the targeted tumors and their microenvironment, with a relative sparing of the adjacent liver parenchyma (if non-ablative doses are administered). It appears now that evaluating tumor response only on morphological basis is not sufficient, and can even lead to wrong interpretation of the treatment efficiency. SIRT causes a combination of early embolisation by obliteration of neoformed arterioles, and local beta-emitting radiation, which is the major component of the therapy. The radiotherapy effectiveness is delayed and first morphological changes such as volume variations or necrosis are observed about 8 to 12 weeks after treatment (related to the tumor absorbed dose and its radiotherapy sensitivity) [58] while functional and metabolic changes can occur earlier. Moreover, SIRT can induce intratumoral inflammation and haemorrhage and oedema peripheral to treated lesions, which can complicate the analysis by morphological criteria on contrast-enhanced imaging (CT or MRI).

The SIRT efficacy should therefore be assessed using morphological and functional or metabolic characteristics [59]. It must be kept in mind that for accurate response assessment the same imaging modality should be performed for both baseline and post-SIRT imaging, in identical and standardized conditions.

Morphological changes: Morphological response on CT and MRI is classically assessed according to the RECIST criteria [60], which were revised in 2009 (RECIST 1.1), or to the WHO criteria [61]. Those criteria consist in evaluating variations of the maximal diameters of the lesions measured in a transverse plan, with measurement of the longest diameters for RECIST and of the two longest perpendicular diameters for WHO.

However, these criteria are criticised because of lack of sufficient correlation with the evolution of the metabolic activity on the FDG PET-CT, which is considered as a more sensitive technique in response assessment of secondary liver tumours, particularly if treated by loco-regional treatments [62]. The lack of accuracy of RECIST is due to the development of necrotic, oedematous or hemorrhagic changes after SIRT, causing paradoxal increase of the dimensions in responding lesions. A certain amount of response is underevaluated, in particular in liver showing parenchyma alterations due to previous surgery, chemotherapy or loco-regional treatments [63,64]. On CT and MRI, lesions are delineated on basis of contrast gradients between tumor and normal parenchyma. Improved spatial resolution (<1mm) and the development of dedicated software have lead to isometric acquisitions, which permit three-dimensional reconstructions and the volumetric evaluation of lesions. It should be expected that this could improve the sensitivity of the detection of change. Nevertheless, lesion volumetric changes have not yet been proved to be more accurate than RECIST or WHO for the response assessment of liver tumours treated by SIRT [65].

Other morphological changes have been proposed for assessing response after vascular interventional therapies and radiofrequency ablation. For instance, the EASL criteria for the HCC, propose the assessment of response by CT or MRI four weeks after treatment with measurements of the diameter of viable tumour as identified by areas of enhancement rather than tumour size [66]. However, measuring areas of enhancement seems to difficult to standardize, leading to low reproducibility. Other morphological changes than tumor measurements may occur earlier and could be correlated with functional changes and tumor response. In 2004, Choi et al. [67] proposed to evaluate attenuation changes of the lesions on CECT for the response assessment of Gastro-Intestinal Stromal Tumours (GIST) after targeted therapy by imatinib mesylate, showing a better correlation of this parameter with the metabolic response on FDG PET, compared to classical RECIST criteria [67,68]. The drop of Hounsfiel

Units (HU) is related to the loss of lesion X-ray attenuation secondary to the loss of cellular density which is closely related to tumor response. For colorectal cancer liver metastasis, other studies demonstrated that the variation of density inside the lesions on CECT, with response defined as a ≥10% of decrease in HU compared to baseline imaging, correlates with the metabolic response on FDG-PET CT [69,70]. However, a major issue remains the delineation of the baseline and residual lesion volumes wherein the mean HUs should be assessed. The response post SIRT can be very heterogeneous within the lesion itself yielding a mix of responding, non-responding, fibrotic and necrotic tumor parts. In our experience with colorectal liver metastasis response evaluation post SIRT using HU based criteria is only accurate with the help of co-registered FDG PET-CT on which the residual viable tumor lesion is easily delineated. Further studies are awaited which will more precisely define the relative role of these HU- based methods in the SIRT evaluation.

Functional changes: Diffusion-weighted MRI (DW-MRI) : Diffusion-weighted MRI, exploring diffusion of water molecules, can depict early changes in the lesion environment and should therefore be considered as an alternative to CECT. Increased tumour tissue water mobility after therapy is presumed to correspond to decreased cellularity, cell size changes (ie, shrinkage), and compromised cell membrane integrity [71].

Moreover, DWI-MRI allows quantitative information by measurements of the ADC (Apparent Diffusion Coefficient). In tumours, high cellular density and oedema cause a restriction of diffusion of water molecules, which is expressed by lowered ADC values on DW-MRI. After treatment, due to hemorrhagic and necrotising patterns, with lyses of cellular membranes and increased extracellular space, water diffusion is facilitated and ADC values are increased. Electromagnetic gradients are applied in the 3 planes of space and are included in echo planar sequences. The value of these gradients is called "b-values" and its unit is s/mm^2. At least two diffusion imaging acquisitions are needed for the calculation of the ADC (mm^2/s), using a sequence without and with diffusion weighting (b=0 and b>0).

ADC calculation can provide a diffusion mapping, but also a perfusion study of microvessels if a large range of b values (b = 0, 50, 100, 150, 200, 250, 300, 500, 750 and 1,000 s/mm^2) is used. If restricted to low be-values (<100) this method may give some information on tissue perfusion, while ADC calculated using the higher b-values (e.g. b = 500, 750, 1,000 s/mm^2) shows mainly diffusion effects. The application of high b-values may reduce the influence of perfusion and may approximate true diffusion [72].

ADC values calculations, using echo planar imaging (EPI) sequences, may be different following to the sampling methodology (size of the ROI, inclusion of necrosis or not…) and the parameters of used sequences. Moreover, lesion location and size are potentially influential on the reproducibility of ADC measurement [73]. ADC measurements in respiratory- triggered DWI are significantly higher and less reproducible than in breath-hold and free-breathing DWI [74].

Diffusion changes in tumours after SIRT are quickly observed [75,76]. For instance, lowered ADC values are seen for HCC after 1 month [77,78]. Recent studies on response after TACE for HCC showed significant ADC values changes after 1-2 weeks and even after 24 hours, correlating with contrast enhancement reduction on MRI [79]. A significant increase in the ADC values following TACE in patients with HCC could be seen as early as 12–24 h after treatment in patients who were subsequently defined as responders by RECIST criteria [80]. However, there is still a lack of evidence of correlation between ADC increase and lowered tumoral marker and prolonged time to progression/survival.

The most pertinent time point for DWI-MRI after SIRT is still not defined and will require prospective trials with measurements at multiple time points after SIRT and using lesion based follow up as the reference.

In conclusion, more studies are needed to validate the use of DW-MRI for the prediction of SIRT response. A major issue is that harmonisation and standardisation of the methodology is still evolving, which is a prerequisite for the technique to be used in prospective multicentric trials.

Metabolic and molecular changes: FDG PET-CT: Positron emission tomography, imaging different metabolic and molecular pathways of biological tissues, is gaining importance in the response assessment after SIRT. Advantages of the PET are its whole body field of view assessing the response and evolution of all hepatic and extra-hepatic lesions in one single imaging session, and the precocity of metabolic tumour changes detected after treatment application. Moreover, different metabolic pathways of tumour cells can be imaged, thanks to different radiolabelled tracers (see higher).

The use of FDG-PET for response assessment after SIRT is based upon a loss of GLUT expression secondary to the treatment induced loss of cellularity and of cellular dysfunction.

It is generally performed at baseline (less that 2-3 weeks before SIRT) and at 6-8 weeks after SIRT. It is not clear whether more early PET response could be applied, eg. at two weeks after SIRT. Theoretically, this would be preferred because more rapid treatment adaptation would thus become possible (see also chapter on post treatment imaging). (Figure 12) shows an example of a FDG PET response measured at 6 weeks and at 3 months, indicating that at 6 weeks the majority of response is measured.

FDG PET-CT should be systematically performed in case of highly glucose-avid neoplasms such as colo-rectal cancer, breast cancer metastasis, (ocular) melanoma and (most cases of) cholangiocarcinoma. For these indications, a significant decrease of the FDG uptake has been observed, predicting the outcome of the patients in terms of disease free survival [81-83].

A study performed by our group has found a significant correlation between the pre SIRT 99mTc-MAA uptake (which is predictive for the amount of activities deposited in the tumor, and, thus, for the tumor absorbed dose) and the FDG PET based metabolic response in colorectal cancer liver metastases [49].

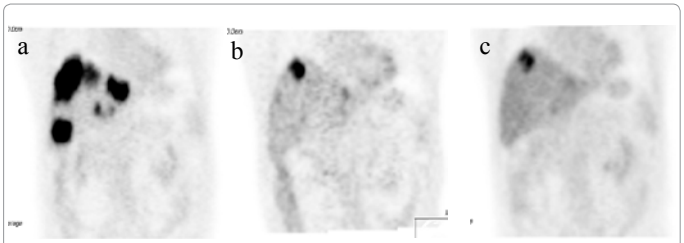

Figure 12: Registered coronal image of a baseline PET (a), 6 week (b) and 3 months (c) after SIRT. This set of images shows the intra-individual variability of the lesion-based metabolic responses seen after SIRT (with one lesion showing a non-response), and, that response at 6 weeks is almost completely similar than the one measured at 3 months.

The same study was also the first to demonstrate that SIRT response was very variable among patients but also within the same patient (Figure 5). It was found that this inter- and intra-individual response variability was strongly depending on the lesion-based radiation absorbed dose, which was well enough predicted by the 99mTc-MAA uptake measure by SPECT-CT during the pre SIRT simulation phase. This strongly emphasizes the clinical need for the use of lesion-based response predictive models such as the predictive dosimetry based upon the 99mTc-MAA distribution, as discussed higher.

As mentioned before, other metabolic markers than ^{18}F-FDG could be proposed for low or inconsistent FDG uptake tumours, such as Ga68-labeled octreotide for neuroendocrine tumours or 18F-fluorocholine for HCC, but further studies should be conducted in order to examine and validate their role for response assessment. A major issue in the use of Ga68-labeled octreotide is the theoretical fact that after SIRT the tracer tumor uptake can decrease both as a result of a loss of cell number as due to a change in receptor expression intensity induced by the radiotherapy itself.

References

1. King J, Quinn R, Glenn DM, Janssen J, Tong D, et al. (2008) Radioembolization with selective internal radiation microspheres for neuroendocrine liver metastases. Cancer 113: 921-929.
2. Kennedy AS, Salem R (2010) Radioembolization (Yttrium-90 Microspheres) for Primary and Metastatic Hepatic Malignancies. Cancer J 16: 163-175.
3. Gonsalves CF, Eschelman DJ, Sullivan KL, Anne PR, Doyle L, et al. (2011) Radioembolization as Salvage Therapy for Hepatic Metastasis of Uveal Melanoma: A Single-Institution Experience. Am J Roentgenol 196: 468-473.
4. Lonneux M, Reffad AM, Detry R, Kartheuser A, Gigot JF, et al. (2002) FDG-PET improves the staging and selection of patients with recurrent colorectal cancer. Eur J Nucl Med Mol Imaging 29: 915-921.
5. Squillaci E, Manenti G, Mancino S, Cicciò C, Calabria F, et al. (2008) Staging of colon cancer: whole-body MRI vs. whole-body PET-CT—initial clinical experience. Abdom Imaging 33: 676-688.
6. Selzner M, Hany TF, Wildbrett P, McCormack L, Kadry Z, et al. (2004). Does the Novel PET/CT Imaging Modality Impact on the Treatment of Patients With Metastatic Colorectal Cancer of the Liver? Ann Surg 240: 1027-1034.
7. Abel-Nabi H, Doerr RJ, Lamonica DM, Cronin VR, Galantowicz PJ, et al. (1998) Staging of primary colorectal carcinomas with fluorine-18 fluorodexoyglucose whole-body PET: correlation with histopathologic and CT findings. Radiology 206: 755-760.
8. Nahas CSR, Akhurst T, Yeung H, Leibold T, Riedel E, et al. (2007) Positron emission tomography detection of distant metastatic or synchronous disease in patients with locally advanced rectal cancer receiving preoperative chemoradiation. Ann Surg Oncol 15: 704-711.
9. Bruegel M, Rummeny EJ (2009) Hepatic metastases: use of diffusion-weighted echo-planar Imaging. Abdom Imaging 35: 454-461.
10. Muhi A, Ichikawa T, Motosugi U, Sou H, Nakajima H, et al. (2010) Diagnosis of colorectal hepatic metastases: Contrast-enhanced ultrasonography versus contrast-enhanced computed tomography versus superparamagnetic iron oxide-enhanced magnetic resonance imaging with diffusion-weighted Imaging. J Magn Reson Imaging 32: 1132-1140.
11. Cantwell CP, Setty B, Holalkere N, Sahani D, Fischman AJ, et al. (2008) Liver Lesion Detection and Characterization in Patients With Colorectal Cancer: A Comparison of Low Radiation Dose Non-enhanced PET/CT, Contrast-enhanced PET/CT, and Liver. MRI J Comput Assist Tomogr 32: 738-744.
12. Rappeport ED, Loft A (2007) Liver metastases from colorectal cancer: imaging with superparamagnetic iron oxide (SPIO)-enhanced MR imaging, computed tomography and positron emission tomography. Abdom Imaging 32 : 624-634.
13. Ward J, Robinson PJ, Guthrie JA, Downing S, Wilson D, et al. (2005) Liver Metastases in Candidates for Hepatic Resection: Comparison of Helical CT and Gadolinium- and SPIO-enhanced MR Imaging. Radiology 237: 170-180.
14. Yoon KT, Kim JK, Kim do Y, Ahn SH, Lee JD, et al. (2007) Role of 18F fluorodeoxyglucose positron emission tomography in detecting extrahepatic metastasis in pretreatment staging of hepatocellular carcinoma. Oncology 72: 104-110.
15. Cho H, Cho A, Kim T, Kang W, Lee J, et al. (2008) 18F-FDG PET/CT in the detection of extrahepatic metastases from hepatocellular carcinoma. J Nucl Med 49: 250.
16. Clark HP, Carson WF, Kavanagh PV, Ho CP, Shen P, et al. (2005) Staging and Current Treatment of Hepatocellular Carcinoma. Radiographics 25: S3-S23.
17. Marrero JA, Kudo M, Bronowicki JP (2010) The Challenge of Prognosis and Staging for Hepatocellular Carcinoma. Oncologist 15: 23-33.
18. Krinsky GA, Lee VS, Theise ND, Weinreb JC, Rofsky NM, et al. (2001) Hepatocellular carcinoma and dysplastic nodules in patients with cirrhosis: prospective diagnosis with MR imaging and explantation correlation. Radiology 219: 445-454.
19. Krinsky GA, Lee VS, Theise ND, Weinreb JC, Rofsky NM, et al. (2002) Transplantation for hepatocellular carcinoma and cirrhosis: sensitivity of magnetic resonance imaging. Liver Transpl 8: 1156-1164.
20. Willatt JM, Hussain HK, Adusumilli S, Marrero JA (2008) MR Imaging of Hepatocellular Carcinoma in the Cirrhotic Liver: Challenges and Controversies. Radiology 247: 311-330.
21. Vandecaveye V, De Keyzer F, Verslype C, Op de Beeck K, Komuta M, et al. (2009) Diffusion-weighted MRI provides additional value to conventional dynamic contrast-enhanced MRI for detection of hepatocellular carcinoma. Eur Radiol 19: 2456-2466.
22. Cher HT, Su-Chong AL, and Choon Hua T (2011) APASL and AASLD Consensus Guidelines on Imaging Diagnosis of Hepatocellular Carcinoma: A Review. Intern J Hepat.
23. Xu PJ, Yan FH, Wang JH, Lin J, and Ji Y (2009) Added value of breathhold diffusion-weighted MRI in detection of small hepatocellular carcinoma lesions compared with dynamic contrast-enhanced MRI alone using receiver operating characteristic curve analysis. J Magn Reson Imaging 2: 341-349.
24. Talbot JN, Fartoux L, Balogova S, Nataf V, Kerrou K, et al. (2010) Detection of hepatocellular carcinoma with PET/CT: a prospective comparison of 18F-fluorocholine and 18F-FDG in patients with cirrhosis or chronic liver disease. J Nucl Med 51: 1699-1706.
25. Luboldt W, Hartmann H, Wiedemann B, Zöphel K, Luboldt HJ (2010) Gastroenteropancreatic neuroendocrine tumors: standardizing therapy monitoring with 68Ga-DOTATOC PET/CT using the example of somatostatin receptor radionuclide therapy. Mol Imaging 9: 351-358.
26. Bal CS, Gupta SK, Zaknun JJ (2010) Radiolabeled somatostatin analogs for radionuclide imaging and therapy in patients with gastroenteropancreatic neuroendocrine tumors. Trop Gastroenterol 31: 87-95.
27. Kayani I, Bomanji JB, Groves A, Conway G, Gacinovic S, et al. (2008). Functional imaging of neuroendocrine tumors with combined PET/CT using ^{68}Ga-DOTATATE (DOTA-DPhe^{1},Tyr^{3}-octreotate) and ^{18}F-FDG. Cancer 112: 2447-2455.
28. Belhocine T, Foidart J, Rigo P, Najjar F, Thiry A, et al. (2002). Fluorodeoxyglucose positron emission tomography and somatostatin receptor scintigraphy for diagnosing and staging carcinoid tumours: correlations with the pathological indexes p53 and Ki-67. Nucl Med Commun 23: 727-734.
29. Slattery JM, Sahani DV (2006) What is the current state- of-the-art imaging for detection and staging of cholangiocarcinoma? Oncologist 11: 913-922.
30. Lee HY, Kim SH, Lee JM, Kim SW, Jang JY, et al. (2006) Preoperative assessment of resectability of hepatic hilar cholangiocarcinoma: combined CT and cholangiography with revised criteria. Radiology 239: 113-121.
31. Sainani NI, Catalano OA, Holalkere NS, Zhu AX, Hahn PF, et al. (2008). Cholangiocarcinoma: Current and Novel Imaging Techniques. Radiographics 28: 1263-1287.
32. Ruys AT, Bennink RJ, van Westreenen HL, Engelbrecht MR, Busch OR, et al. (2011) FDG-positron emission tomography/computed tomography and standardized uptake value in the primary diagnosis and staging of hilar cholangiocarcinoma. HPB (Oxford) 13: 256-262.
33. Kim YJ, Yun M, Lee WJ, Kim KS, Lee JD (2003) Usefulness of 18F-FDG PET in intrahepatic cholangiocarcinoma. Eur J Nucl Med Mol Imaging 30: 1467-1472.
34. Fritscher-Ravens A, Bohuslavizki KH, Broering DC, Jenicke L, Schäfer H, et

al. (2001) FDG PET in the diagnosis of hilar cholangiocarcinoma. Nucl Med Commun 22: 1277-1285.

35. Sahani D, Mehta A, Blake M, Prasad S, Harris G, et al. (2004) Preoperative Hepatic Vascular Evaluation with CT and MR Angiography: Implications for Surgery. Radiographics 24: 1367-1380.

36. Sahani D, Saini S, Nichols S, Nichols S, Prasad SR, et al. (2002) Using multidetector CT for preoperative vascular evaluation of liver neoplasms: technique and results. AJR Am J Roentgenol 179: 53-59.

37. Prokop M, (2000) Multislice CT angiography. Eur J Radiol 36: 86-96.

38. Taguchi K, Anno H (2000) High temporal resolution for multislice helical computed tomography. Med Phys 27: 861-872.

39. Chan JK, Tso WK, Lo CM, Fan ST, Chan KL, et al. (1998) Preoperative evaluation of potential living donors for liver transplantation: the role of helical computed tomography-angiography. Transplant Proc 30: 3197-3198.

40. Pannu HK, Maley WR, Fishman EK (2001) Liver transplantation: preoperative CT evaluation. RadioGraphics 21: S133-S146.

41. Laghi A (2007) Multidetector CT (64 Slices) of the liver: examination techniques. Eur Radiol 17: 675-683.

42. Sone M, Kato K, Hirose A, Nak asato T, Tomabechi M, et al. (2008) Impact of Multislice CT Angiography on Planning of Radiological Catheter Placement for Hepatic Arterial Infusion Chemotherapy Cardiovasc Intervent Radiol 31: 91-97.

43. Sahani D, Mehta A, Blake M, Prasad S, Harris G, et al. (2004) Preoperative Hepatic Vascular Evaluation with CT and MR Angiography: Implications for Surgery. Radiographics 24: 1367-1380.

44. Lee MW, Lee JM, Lee JY, Kim SH, Park EA, et al. (2006). Preoperative evaluation of the hepatic vascular anatomy in living liver donors: Comparison of CT angiography and MR angiography. J Magn Reson Imaging 24: 1081-1087.

45. Virmani S, Ryu RK, Sato KT, Lewandowski RJ, Kulik L, et al. (2007) Effect of C-arm angiographic CT on transcatheter arterial chemoembolization of liver tumors. J Vasc Interv Radiol 18: 1305-1309.

46. Liapi E, Hong K, Georgiades CS, Geschwind JF (2005) Three-dimensional rotational angiography: introduction of an adjunctive tool for successful transarterial chemoembolization. J Vasc Interv Radiol 16: 1241-1245.

47. Bridcut RR, Murphy E, Workman A, Flynn P, Winder RJ (2007) Patient dose from 3D rotational neurovascular studies. Br J Radiol 80: 362-366.

48. Murthy R, Brown DB, Salem R, Meranze SG, Coldwell DM et al. (2007) Gastrointestinal Complications Associated with Hepatic Arterial Yttrium-90 Microsphere Therapy. J Vasc Interv Radiol 8: 553-561.

49. Lin M (1994) Radiation pneumonitis caused by yttrium-90 microspheres: radiologic findings. Am J Roentgenol 162: 1300-1302.

50. Louie JD, Kothary N, Kuo WT, Hwang GL, Hofmann LV, et al. (2009) Incorporating Cone-beam CT into the Treatment Planning for Yttrium-90 Radioembolization. J Vasc Interv Radiol 20: 606-613.

51. Chiesa C, Maccauro M, Romito R, Spreafico C, Pellizzari S, et al. (2011) Need, feasibility and convenience of dosimetric treatment planning in liver selective internal radiation therapy with 90Y microspheres: the experience of the National Tumor Institute of Milan. Q J Nucl Med Mol Imaging 55: 168-197.

52. Asseler Y (2009) Advances in SPECT imaging with respect to radionuclide therapy. Q J Nucl Med Mol Imaging 53: 343-347.

53. Giammarile F, Bodei L, Chiesa C, Flux G, Forrer F, et al. (2011) EANM procedure guideline for the treatment of liver cancer and liver metastases with intra-arterial radioactive compounds. Eur J Nucl Med Mol Imaging 38: 1393-1406.

54. Flamen P, Vanderlinden B, Delatte P, Ghanem G, Ameye L, et al. (2008) Multimodality imaging can predict the metabolic response of unresectable colorectal liver metastases to radioembolization therapy with Yttrium-90 labeled resin microspheres Phys Med Biol 53: 6591-6603.

55. Shen S, DeNardo GL, Yuan A, DeNardo DA, DeNardo SJ (1994) Planar gamma camera imaging and quantitation of yttrium-90 bremsstrahlung. J Nucl Med 35: 1381-1389.

56. Shen S, DeNardo GL, DeNardo SJ (1994) Quantitative bremsstrahlung imaging of yttrium-90 using a Wiener filter. Med Phys 21:1409-1417.

57. Ito S, Kurosawa H, Kasahara H, Teraoka S, Ariga E, et al.(2009) 90Y bremsstrahlung emission computed tomography using gamma cameras. Ann Nucl Med 23: 257-267.

58. Minarik D, Sjögreen Gleisner K, Ljungberg M (2008) Evaluation of quantitative (90)Y SPECT based on experimental phantom studies. Phys Med Biol 53: 5689-5703.

59. Fabbri C, Sarti G, Cremonesi M, Ferrari M, Di Dia A, et al. (2009) Quantitative analysis of 90Y Bremsstrahlung SPECT-CT images for application to 3D patient-specific dosimetry. Cancer Biother Radiopharm 24: 145-154.

60. Selwyn RG, Nickles RJ, Thomadsen BR, DeWerd LA, Micka JA (2007) A new internal pair production branching ratio of 90Y: the development of a non-destructive assay for 90Y and 90Sr. Appl Radiat Isot 65: 318-327.

61. Lhommel R, Goffette P, Van den Eynde M, Jamar F, Pauwels S, et al. (2009) Yttrium-90 TOF PET scan demonstrates high-resolution biodistribution after liver SIRT. Eur J Nucl Med Mol Imaging 36: 1696.

62. Lhommel R, van Elmbt L, Goffette P, Van den Eynde M, Jamar F, et al. (2010) Feasibility of 90Y TOF PET-based dosimetry in liver metastasis therapy using SIR-Spheres. Eur J Nucl Med Mol Imaging 37: 1654-1662.

63. Salem R, Lewandowski RJ, Atassi B, Gordon SC, Gates VL, et al. (2005) Treatment of unresectable hepatocellular carcinoma with use of 90Y microspheres (TheraSphere): safety, tumor response, and survival. J Vasc Interv Radiol 16: 1627-1639.

64. Atassi B, Bangash AK, Bahrani A, Pizzi G, Lewandowski RJ, et al. (2008) Multimodality Imaging Following ^{90}Y Radioembolization: A Comprehensive Review and Pictorial Essay. Radiographics 28: 81-99.

65. Eisenhauer EA, Therasse P, Bogaerts J, Schwartz LH, Sargent D, et al. (2009). New response evaluation criteria in solid tumours: Revised RECIST guideline (version 1.1). Eur J Cancer 45 : 228-247.

66. Miller AB, Hoogstraten B, Staquet M, Winkler A (1981) Reporting results of cancer treatment. Cancer 47: 207-214.

67. Dierckx R, Maes A, Peeters M, Van de Wiele C (2009) FDG PET for monitoring response to local and locoregional therapy in HCC and liver metastases. Q J Nucl Med Mol Imaging 53: 336-342.

68. Suzuki C, Jacobsson H, Hatschek T, Torkzad MR, Bodén K, et al. (2008) Radiologic measurements of tumor response to treatment: practical approaches and limitations. Radiographics 28: 329-344.

69. Liapi E, Geschwind JF, Vossen JA, Buijs M, Georgiades CS, et al. (2008) Functional MRI evaluation of tumor response in patients with neuroendocrine hepatic metastasis treated with transcatheter arterial chemoembolization. AJR Am J Roentgenol 190: 67-73.

70. Wong C, Salem R, Raman S, Gates VL, Dworkin HJ, et al. (2002) Evaluating 90Y-glass microsphere treatment response of unresectable colorectal liver metastases by [18F]FDG PET: a comparison with CT or MRI. EJNMMI 29: 815-820.

71. Bruix J, Sherman M, Llovet JM, Beaugrand M, Lencioni R, et al. (2001) Clinical management of hepatocellular carcinoma. Conclusions of the Barcelona- 2000 EASL conference. European Association for the Study of the Liver. J Hepatol 35: 421-430.

72. Choi H, Charnsangavej C, de Castro Faria S, Tamm EP, Benjamin RS, et al. (2004) CT evaluation of the response of gastrointestinal stromal tumors after imatinib mesylate treatment: a quantitative analysis correlated with FDG PET findings. AJR AM J Roentgenol 183: 1619-1628.

73. Choi H, Charnsangavej C, Faria SC, Macapinlac HA, Burgess MA, et al. (2007) Correlation of computed tomography and positron emission tomography in patients with metastatic gastrointestinal stromal tumor treated at a single institution with imatinib mesylate: proposal of new computed tomography response criteria. J Clin Oncol 25: 1753-1759.

74. Tochetto SM, Rezai P, Rezvani M, Nikolaidis P, Berggruen S, et al. (2010) Does multidetector CT attenuation change in colon cancer liver metastases treated with 90Y help predict metabolic activity at FDG PET? Radiology 255: 164-172.

75. Miller FH, Keppke AL, Reddy D, Huang J, Jin J, et al. (2007) Response of Liver Metastases After Treatment with Yttrium-90 Microspheres: Role of Size, Necrosis, and PET. Am J Roentgenol 188: 776-783.

76. Le Bihan D, Breton E, Lallemand D, Aubin ML, Vignaud J, et al. (1988) Separation of diffusion and perfusion in intravoxel incoherent motion MR imaging. Radiology 168: 497-505.

77. Thoeny HC, De Keyzer F, Chen F, Ni Y, Landuyt W, et al. (2005) Diffusion-weighted MR imaging in monitoring the effect of a vascular targeting agent on rhabdomyosarcoma in rats. Radiology 234: 756-764.

78. Kim SY, Lee SS, Byun JH, Park SH, Kim JK, et al. (2010) Malignant Hepatic Tumors: Short-term Reproducibility of Apparent Diffusion Coefficients with Breath-hold and Respiratory-triggered Diffusion-weighted MR Imaging. Radiology 255: 815-823.

79. Kwee TC, Takahara T, Koh DM, Nievelstein RA, Kuijten PR (2008) Comparison and reproducibility of ADC measurements in breathhold, respiratory triggered, and free breathing diffusion-weighted MR imaging of the liver. Magn Reson Imaging 28: 1141-1148.

80. Liapi E, Kamel IR (2010) DW-MRI Assessment of Treatment Response to Minimally Invasive Therapy. Medical Radiology 3: 175-185.

81. Dudeck O, Zeile M, Wybranski C, Schulmeister A, Fischbach F, et al. (2010) Early prediction of anticancer effects with diffusion-weighted MR imaging in patients with colorectal liver metastases following selective internal radiotherapy. Eur Radiol 11: 2699-2706.

82. Rhee TK, Naik NK, Deng J, Atassi B, Mulcahy MF, et al. (2008) Tumor response after yttrium-90 radioembolization for hepatocellular carcinoma: comparison of diffusion-weighted functional MR imaging with anatomic MR imaging. Journal of Vascular and Interventional Radiology 19:1180-1186.

83. Kamel IR, Reyes DK, Liapi E, Bluemke DA, Geschwind JF (2007) Functional MR imaging assessment of tumor response after 90Y microsphere treatment in patients with unresectable hepatocellular carcinoma. J Vasc Interv Radiol 18: 49-56.

84. Deng J, Miller FH, Rhee TK, Sato KT, Mulcahy MF, et al. (2006) Diffusion-weighted MR Imaging for Determination of Hepatocellular Carcinoma Response to Yttrium-90 Radioembolization. J Vasc Interv Radiol 17: 1195-1200.

85. Kamel I, Liapi E, Reyes D, Zahurak M, Bluemke DA, et al. (2009) Unresectable hepatocellular carcinoma: serial early vascular and cellular changes after transarterial chemoembolization as detected with MR imaging. Radiology 250: 466-473.

86. Haug AR, Heinemann V, Bruns CJ, Hoffmann R, Jakobs T, et al. (2011) 18F-FDG PET independently predicts survival in patients with cholangiocellular carcinoma treated with 90Y microspheres. EJNMMI, Online First™, 10 February 2011.

87. Bienert M, McCook B, Carr BI, Geller DA, Sheetz M, et al. (2005) 90Y microsphere treatment of unresectable liver metastases: changes in 18F-FDG uptake and tumour size on PET/CT. Eur J Nucl Med Mol Imaging 32: 778-787.

88. Szyszko T, AL-Nahhas A, Canelo R, Habib N, Jiao L, et al. (2007) Assessment of response to treatment of unresectable liver tumours with 90Y microspheres: Value of FDG PET versus computed tomography. Nucl Med Commun 28: 15-20.